Photodissociation of O_2 via the Herzberg continuum: Measurements of O-atom alignment and orientation

Andrew J. Alexander,[a] Zee Hwan Kim,[b] and Richard N. Zare[c]
Department of Chemistry, Stanford University, Stanford, California 94305-5080

(Received 29 January 2003; accepted 24 March 2003)

Irradiation of molecular oxygen O_2 in the region of the Herzberg continuum between 218 nm and 239 nm results in the production of open-shell photofragments $O(^3P)+O(^3P)$. Product $O(^3P_j;\ j=0,1,2)$ atoms were ionized using resonantly enhanced multiphoton ionization (2+1 REMPI) near 225 nm and the ions collected in a velocity-sensitive time-of-flight mass spectrometer. By controlling the polarization of the photolysis and ionization radiation, we have measured alignment and orientation parameters of O-atom electronic angular momentum ($\boldsymbol{j}$) in the molecule frame. The results show alignment from both parallel and perpendicular transitions that are cylindrically symmetric about the velocity ($\boldsymbol{v}$) of the recoiling O atom. We also observe electronic alignment that is noncylindrically symmetric about $\boldsymbol{v}$, resulting from coherence between multiply excited dissociative states. Photodissociation with linearly polarized light is shown to produce O atoms that are *oriented* in the molecule frame, resulting from interference between parallel and perpendicular dissociative states of O_2. Semiclassical calculations that include spin–orbit coupling between six excited states reproduce closely the observed polarization. © *2003 American Institute of Physics.* [DOI: 10.1063/1.1574511]

I. INTRODUCTION

Oxygen plays a key role in the chemistry of the Earth's atmosphere. The splitting of the oxygen bond by ultraviolet (UV) solar radiation is the primary step in the formation of ozone (O_3), and is responsible for the existence of the ozone layer.[1] The UV photodissociation of O_2 can be loosely classed in three different wavelength regions: the Herzberg continuum (242–200 nm), the Schumann–Runge bands (200–176 nm), and the Schumann–Runge continuum (176–100 nm).

The Herzberg continuum is the region of near-threshold dissociation of O_2 to give $O(^3P)+O(^3P)$. The electronic configuration of the O atoms ($1s^2 2s^2 2p^4$) leads to a considerable number of electronic states of the O_2 molecule, and a ground state $X\ ^3\Sigma_g^-$ that is unusual in that it has two unpaired electrons. In the Herzberg continuum, absorption occurs from the X state to the $A\ ^3\Sigma_u^+$, $A'\ ^3\Delta_u$, and $c\ ^1\Sigma_u^-$ states: these are called the Herzberg I, II, and III transitions respectively. These Herzberg transitions are electric dipole forbidden, and the absorption cross sections (σ) are weak: for example, $\sigma \approx 10^{-24}$ cm^2 at 240 nm.[2] Oscillator strength for the Herzberg transitions is borrowed from electric dipole allowed transitions, mainly through spin–orbit (SO) interactions between ground and excited states. Buijsse *et al.*,[3] have recently published results of a detailed velocity-map imaging study of photodissociation in the Herzberg continuum. The velocity map experiments measured the directions of velocities of the product O atoms with respect to the electric field vector $\boldsymbol{\epsilon}$ of the linearly polarized photolysis radiation. The angular distribution can be written using the expression[4]

$$I(\theta_\epsilon)=\frac{1}{4\pi}[1+\beta P_2(\cos\ \theta_\epsilon)], \tag{1}$$

where $P_2(\cdots)$ is the second order Legendre polynomial, θ_ϵ is the polar angle between $\boldsymbol{v}$ and $\boldsymbol{\epsilon}$, and the spatial distribution of velocities is parameterized by β. The β parameter takes the limits $+2$ for a parallel ($\parallel$) transition and -1 for a perpendicular ($\perp$) transition. At 226 nm, $\beta=0.61$ for $O(^3P_2)$, indicating a mixture of 54% ($\parallel$) with 46% ($\perp$). Buijsse *et al.* have developed a detailed photoabsorption model to directly compare with the experimental results. The Herzberg I transition was found to be the most significant, accounting for 86% of the total cross section at 242 nm, and rising to 94% at 198 nm. The resulting electric dipole transition includes both parallel and perpendicular components

$$X\ ^3\Sigma_{g,\pm1}^- \overset{\parallel}{\rightarrow} B\ ^3\Sigma_{u,\pm1}^- \overset{\mathrm{SO}}{\leftrightarrow} A\ ^3\Sigma_{u,\pm1}^+, \tag{2}$$

$$X\ ^3\Sigma_{g,0+}^- \overset{\mathrm{SO}}{\leftrightarrow} 1\ ^3\Pi_{g,0+} \overset{\perp}{\rightarrow} A\ ^3\Sigma_{u,\pm1}^+, \tag{3}$$

$$X\ ^3\Sigma_{g,\pm1}^- \overset{\mathrm{SO}}{\leftrightarrow} 1\ ^3\Pi_{g,\pm1} \overset{\perp}{\rightarrow} A\ ^3\Sigma_{u,0-}^-. \tag{4}$$

Here, we have given the projection $\Omega\equiv\Lambda+\Sigma$ of total angular momentum on the bond axis as an additional subscript on the term symbol, $^{2\Sigma+1}\Lambda_{g/u,\Omega}^{\pm}$. The transitions to $A'\ ^3\Delta_u$ and $c\ ^1\Sigma_u^-$ are purely perpendicular in character.

Adiabatically, the A, A', and c states correlate to give O atoms with $j=2$, i.e., $O(^3P_2)+O(^3P_2)$. Several studies have shown significant populations of $O(^3P_j)$ with $j=0,1$.[5–7]

[a]Present address: School of Chemistry, University of Edinburgh, Edinburgh EH9 3JJ, UK.
[b]Present address: College of Chemistry, University of California, Berkeley CA 94720-1460.
[c]Author to whom correspondence should be addressed. Electronic mail: zare@stanford.edu

Buijsse *et al.*[3] measured the $j=0:1:2$ branching ratio as 1.00:3.33:9.00. Clearly a significant amount of nonadiabatic interaction takes place during the dissociation. There are a total of eight states of ungerade symmetry correlating to the $O(^3P)+O(^3P)$ dissociation limit, these include three Herzberg states (A, A', and c) and five others ($1\,^1\Pi_u$, $1\,^3\Pi_u$, $2\,^3\Sigma_u^+$, $1\,^5\Pi_u$, and $1\,^5\Sigma_u^-$). The ungerade states may couple through long-range SO interaction, and the $A\,^3\Sigma_u^+$ and $2\,^3\Sigma_u^+$ states may also interact by radial derivative coupling due to the radial kinetic energy operator. Unfortunately, angular distribution and branching ratio measurements do not reveal clues to the specific states involved in the nonadiabatic dissociation.

Recently, van Vroonhoven and Groenenboom[8] (VG) calculated *ab initio* potentials for the eight ungerade states, and the SO and radial derivative couplings between them. These potentials were used in semiclassical calculations of the electronic state-resolved branching ratios and $\beta(j)$ parameters as a function of the dissociation energy, and the calculations were compared with the experimental results of Buijsse *et al.*[9] Significantly, VG also calculated electronic state resolved alignment moments $\rho_0^{(k)}(j)$ $(k=2,4;\ j=1,2)$, but at that time no experimental data were available for comparison. The alignment moments are sensitive to nonadiabatic transitions between states, and their experimental determination would provide a useful test of *ab initio* and dynamical calculations.

In this article, we present measurements of electronic orientation and alignment of $O(^3P_j)$ atoms following dissociation *via* the Herzberg continuum in the region 218–239 nm. The O-atom polarization is obtained in terms of molecule frame polarization parameters $\mathbf{a}_q^{(k)}(p)$ that distinguish between atoms produced by parallel ($\parallel$) or perpendicular ($\perp$) transitions, or coherence due to mixed transitions.[10] The measured alignment parameters allow a detailed comparison with the recent semiclassical calculations of VG. The photodissociation of O_2 with linearly polarized light results in production of O atoms that are oriented in the molecule frame. The orientation results from interference between dissociative states of parallel and perpendicular symmetry. The phase-dependent orientation should prove to be a very sensitive test parameter for the shapes of the dissociative potential energy curves for O_2, and the nonadiabatic transitions between states. The paper is arranged as follows: in Sec. II we describe the experiment and extraction of the polarization parameters. The experimental results are presented in Sec. III in comparison with the semiclassical results of VG and our own semiclassical calculations of the interference between excited dissociative states. Conclusions are given in Sec. IV.

II. METHODS

The experimental methods have been described in detail elsewhere,[11,12] and a brief overview is given here. A 1:9 mixture of oxygen (Matheson, 99.9%) and helium was made and expanded into the source region of a Wiley–Mclaren time-of-flight (TOF) mass spectrometer via a pulsed nozzle (General valve, series 9, 0.6 mm orifice) with a backing pressure of ~400 Torr. The O_2 was photolyzed using linearly polarized light in the 218–239 nm wavelength range. The second harmonic (532 nm) of a Nd^{3+}:YAG laser (Continuum PL9020) was used to pump a dye laser (Continuum ND6000, rhodamine 590+610 dye) to produce tunable radiation in the region 550–616 nm, which was doubled to 275–308 nm using a KDP crystal. The resulting doubled light was then mixed with the residual fundamental (1064 nm) of the Nd^{3+}:YAG laser in a second KDP crystal to produce tunable photolysis radiation from 218 to 239 nm. Measurements of product $O(^3P_j;\ j=1,2)$ atom alignment were made at photolysis wavelengths of 221.667 and 237.049 nm; for brevity, we shall refer to these wavelengths as 222 and 237 nm, respectively. Measurements of $O(^3P_2)$ atom orientation were made at several photolysis wavelengths in the range 218.521–238.556 nm. The $O(^3P_j;\ j=0,1,2)$ atom products were ionized by 2+1 REMPI (resonantly enhanced multiphoton ionization) via the $2p^3 4p(^3P_{j'})$ intermediate state using wavelengths of 226.233, 226.059, and 225.656 nm for $j=0$, 1, and 2, respectively. Polarization measurements are not possible for $O(^3P_0)$ because this state has zero total angular momentum. Tuneable probe radiation around 226 nm was produced by frequency doubling the 450 nm output of a second Nd^{3+}:YAG pumped dye laser (Spectra Physics DCR-2A, PDL-3, coumarin 450 dye). The probe and photolysis laser beams were counterpropagated and both loosely focused (+50 cm focal length) to overlap at the center of the pulsed expansion in the TOF. The resulting O^+ ions were collected with the TOF spectrometer operating under velocity-sensitive conditions.[12]

The direction of the linear polarization of the photolysis beam was controlled using a double Fresnel rhomb (Optics For Research), and the direction of the probe linear polarization was switched on a shot-by-shot basis using a photoelastic modulator (Hinds PEM 80) allowing difference measurements to be made very accurately. For the orientation measurements, the probe beam was circularly polarized using a Soleil-Babinet compensator (Special Optics), and was switched between left- and right-circular polarization using the PEM. The experimental geometries used were the same as described by Rakitzis *et al.*[11] The TOF profiles are labeled by their geometry as $\mathbf{I}_G^F$, where F indicates the geometry of the photolysis polarization, and G indicates the geometry of the probe polarization. The laboratory Z axis lies along the TOF direction, and the Y axis lies along the photolysis laser propagation direction. Left and right circular polarization is indicated by L and R respectively. For example, for the $\mathbf{I}_R^X$ profile, the photolysis laser would be linearly polarized along the X axis, with the counterpropagating probe laser being right circularly polarized. For the alignment experiments, a total set of 4 profiles were recorded. These were obtained in two experiments using the PEM to flip the probe laser polarization between the X and Z axes on a shot-by-shot basis: first with the photolysis polarization along X, and second along Z. This gives two pairs of profiles: $\{\mathbf{I}_Z^X, \mathbf{I}_X^X\}$ and $\{\mathbf{I}_Z^Z, \mathbf{I}_X^Z\}$. TOF profiles that are sensitive to the O-atom velocity, but approximately independent of product atom alignment are calculated as $\mathbf{I}_{\rm iso}^Z=\mathbf{I}_Z^Z+2\mathbf{I}_X^Z$ and $\mathbf{I}_{\rm iso}^X=\mathbf{I}_Z^X+2\mathbf{I}_X^X$. TOF pro-

TABLE I. Interpretation and range of molecule frame polarization parameters $\mathbf{a}_q^{(k)}(p)$ used in the present work. The column headed "Physical Direction" gives the direction of alignment ($k=2$) or orientation ($k=1$) if the parameter is positive (+) or negative (−).

Parameter	Interpretation[a]	Physical direction	Range $j=1$	Range $j=2$
$\mathbf{a}_0^{(2)}(\parallel)$	$c_2\langle 3j_z-j^2\rangle$	(+) $\parallel z$, (−) $\perp z$	$-1.000 \cdots +0.500$	$-1.000 \cdots +1.000$
$\mathbf{a}_0^{(2)}(\perp)$	$c_2\langle 3j_z-j^2\rangle$	(+) $\parallel z$, (−) $\perp z$	$-1.000 \cdots +0.500$	$-1.000 \cdots +1.000$
$\mathrm{Re}[\mathbf{a}_1^{(2)}(\parallel,\perp)]$	$-c_2\sqrt{3/2}\langle j_zj_x+j_xj_z\rangle$	(+) $\parallel x-z$, (−) $\parallel x+z$	$-0.866 \cdots +0.866$	$-1.000 \cdots +1.000$
$\mathbf{a}_2^{(2)}(\perp)$	$c_2\sqrt{3/2}\langle j_x^2-j_y^2\rangle$	(+) $\parallel x$, (−) $\parallel y$	$-0.866 \cdots +0.866$	$-1.000 \cdots +1.000$
$\mathrm{Im}[\mathbf{a}_1^{(1)}(\parallel,\perp)]$	$c_1\sqrt{1/2}\langle j_y\rangle$	(+) $\parallel +y$, (−) $\parallel -y$	$-0.500 \cdots +0.500$	$-0.577 \cdots +0.577$

[a] $c_1=[j(j+1)]^{-1/2}$, $c_2=[j(j+1)]^{-1}$.

files that are sensitive to product atom alignment are calculated as $\mathbf{I}^Z_{\mathrm{aniso}}=\mathbf{I}^Z_Z-\mathbf{I}^Z_X$ and $\mathbf{I}^X_{\mathrm{aniso}}=\mathbf{I}^X_Z-\mathbf{I}^X_X$. In the orientation experiments, the photolysis radiation was polarized at 45° with respect to the TOF axis, along the $(X-Z)$ direction. The probe radiation was switched between left and right circular polarization on a shot-by-shot basis with the PEM to obtain left $\mathbf{I}^{X-Z}_L$ and right $\mathbf{I}^{X-Z}_R$ TOF profiles respectively. Orientation-sensitive and velocity-sensitive composite TOF profiles are defined as $\mathbf{I}^{X-Z}_{\mathrm{aniso}}=\mathbf{I}^{X-Z}_L-\mathbf{I}^{X-Z}_R$ and $\mathbf{I}^{X-Z}_{\mathrm{iso}}=\mathbf{I}^{X-Z}_L+\mathbf{I}^{X-Z}_R$ respectively.[13–16]

Following Rakitzis and Zare,[10] we write the relative (2+1) REMPI intensity I as

$$I[\Theta,\Phi,\theta_\epsilon,\beta,\mathbf{a}_q^k(p)]=1+\beta P_2(\cos\theta_\epsilon)+s_1(j)\sin\theta_\epsilon\cos\theta_\epsilon\,\mathrm{Im}[\mathbf{a}_1^{(1)}(\parallel,\perp)]\sqrt{2}\sin\Theta\sin\Phi+s_2(j)P_2(\cos\Theta)[(1+\beta)\times\cos^2\theta_\epsilon\mathbf{a}_0^{(2)}(\parallel)+(1-\beta/2)\sin^2\theta_\epsilon\mathbf{a}_0^{(2)}(\perp)]+s_2(j)\sin\theta_\epsilon\cos\theta_\epsilon\,\mathrm{Re}[\mathbf{a}_1^{(2)}(\parallel,\perp)]\sqrt{3/2}\times\sin2\Theta\,\cos\Phi+s_2(j)(1-\beta/2)\sin^2\theta_\epsilon\mathbf{a}_2^{(2)}(\perp)\sqrt{3/2}\sin^2\Theta\,\cos2\Phi. \quad (5)$$

Θ,Φ, and θ_ϵ describe the position of the probe and photolysis polarization vectors with respect to the TOF laboratory frame, β is the translational anisotropy parameter, and $\mathbf{a}_q^{(k)}(p)$ are molecule frame polarization parameters. It should be noted that we have multiplied by a factor of $[1+\beta P_2(\cos\theta_\epsilon)]$ that appeared in the denominator of Eq. (16) in Ref. 10. The $s_k(j)$ are (2+1) REMPI polarization sensitivities for $O(^3P_j)$ atoms, and were calculated from the $I_k(j)$ geometrical factors derived by VG,[9] using the conversion

$$s_k(j)=\frac{\sqrt{(2k+1)(2j+1)}[j(j+1)]^{k/2}}{c(k)\langle j\|J^{(k)}\|j\rangle}I_k(j), \quad (6)$$

where $c(1)=1$, $c(2)=\sqrt{6}$ are constants,[13] and the reduced matrix elements $\langle j\|J^{(k)}\|j\rangle$ have been listed elsewhere.[14] Using $I_2(1)=\sqrt{1/2}$ and $I_2(2)=-\sqrt{7/10}$ from VG, we calculate $s_2(1)=1$ and $s_2(2)=-1$. For REMPI by circularly polarized light, it is possible to obtain the sensitivity factor using the simplified expression of Mo and Suzuki,[15] where the $I_k^{\mathrm{SF}}(j_i,j_f)$ of VG are equivalent to P_k of Mo and Suzuki. The calculated P_k can be combined with branching ratios to the excited state as described by VG, and converted to s_k using Eq. (6) above. Orientation measurements were only carried out for $j=2$, for which we calculate $s_1(2)=\sqrt{8/3}$. A prime advantage of measuring polarization of O atoms, is that no hyperfine depolarization occurs because O atoms have zero nuclear spin. On the other hand, experiments that attempt to measure angular distributions of O atoms may be significantly distorted if they do not explicitly account for the effects of polarization on the detection sensitivity.[16]

The molecule frame polarization parameters $\mathbf{a}_q^{(k)}(p)$ are spherical tensor moments of $\boldsymbol{j}$ in the molecule frame,[14] with the z axis being the recoil velocity vector $\boldsymbol{v}$, assuming that the dissociation occurs in the limit of axial recoil. Equation (5) has been derived by rotating the molecule frame into the laboratory (TOF) frame. The $\mathbf{a}_q^{(k)}(p)$ are identified by the symmetry of the parent dipole transition moment (p), which is parallel $(\parallel)$ or perpendicular $(\perp)$ to the diatomic internuclear axis. The symmetry of the transition depends upon the projection of the angular momentum along the O_2 bond axis, Ω. For parallel transitions, the change in the projection of angular momentum is $\Delta\Omega=0$, and for perpendicular transitions $\Delta\Omega=\pm1$.

The interpretations of the $\mathbf{a}_q^{(k)}(p)$ are summarized in Table I. The $\mathbf{a}_0^{(2)}(\parallel)$ and $\mathbf{a}_0^{(2)}(\perp)$ represent cylindrically-symmetric alignment of $\boldsymbol{j}$ about $\boldsymbol{v}$ that arise from incoherent parallel and perpendicular excitations respectively.[17] The parameters $\mathrm{Re}[\mathbf{a}_1^{(2)}(\parallel,\perp)]$ and $\mathrm{Im}[\mathbf{a}_1^{(1)}(\parallel,\perp)]$ arise from the broken cylindrical symmetry of $\boldsymbol{j}$ about $\boldsymbol{v}$ resulting from coherent superposition of parallel and perpendicular excitations. These coherent paramaters vanish in the limit of pure parallel or perpendicular transitions. The $\mathbf{a}_2^{(2)}(\perp)$ results from coherent superposition of perpendicular transitions. The $\mathbf{a}_2^{(2)}(\perp)$ may occur as a result of simultaneous excitation of $|\Omega|=1$ states with different energies, or as a result of the excitation of degenerate $\Omega=\pm1$ components of an $|\Omega|=1$ transition.[17] It should be noted that relationships between $\mathbf{a}_q^{(k)}(p)$ and the dynamical functions $f_k(q,q')$ of Siebbeles *et al.*[17] that appeared in Appendix A of Ref. 10 were incorrect. Correct relationships between the molecule frame pa-

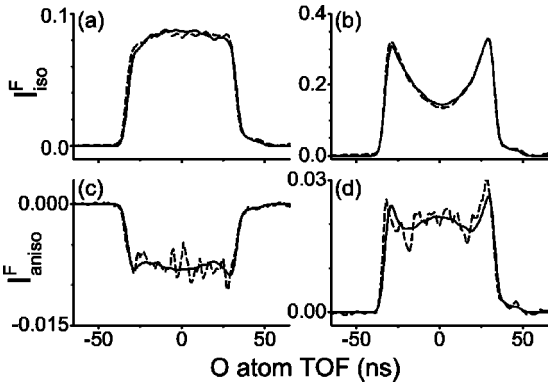

FIG. 1. Isotropic and anisotropic TOF profiles of $O(^3P_2)$ products at photolysis wavelength 222 nm: (a) $\mathbf{I}^X_{iso}$, (b) $\mathbf{I}^Z_{iso}$, (c) $\mathbf{I}^X_{aniso}$, (d) $\mathbf{I}^Z_{aniso}$. Experimental data are shown as dashed lines, fitted data are solid lines.

rameters $\mathbf{a}^{(k)}_q(p)$, the α_k polarization parameters of Vasyutinskii and co-workers,[18] and the dynamical functions of Siebbeles *et al.*[17] have been tabulated by Alexander.[19]

As has been described in detail elsewhere,[10] a set of isotropic and anisotropic basis profiles $\mathbf{B}^F_{iso}$ and $\mathbf{B}^F_{aniso}$ were simulated by Monte Carlo sampling of Eq. (5). The β parameter was varied to produce $\mathbf{B}^F_{iso}$ that gave good fits to the $\mathbf{I}^F_{iso}$,

$$\mathbf{I}^F_{iso} = c^F \mathbf{B}^F_{iso}, \tag{7}$$

where c^F is a weighting coefficient that was subsequently used to fit the anisotropic profiles:

$$\mathbf{I}^F_{aniso} = \sum_{k,q,p} \mathbf{a}^{(k)}_q(p) c^F \mathbf{B}^F_{aniso}. \tag{8}$$

For the alignment experiments, the $F=X$ and $F=Z$ profiles are fitted simultaneously, and the sum in Eq. (8) includes $\mathbf{a}^{(2)}_0(\parallel)$, $\mathbf{a}^{(2)}_0(\perp)$, $\mathrm{Re}[\mathbf{a}^{(2)}_1(\parallel,\perp)]$, and $\mathbf{a}^{(2)}_2(\perp)$. For the orientation experiments, $F=(X-Z)$ and $\mathrm{Im}[\mathbf{a}^{(1)}_1(\parallel,\perp)]$ is the only polarization parameter fitted by Eq. (8).

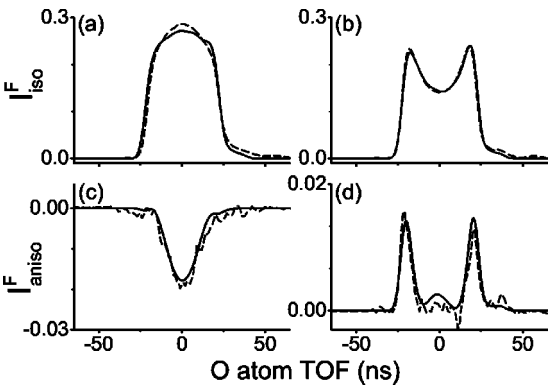

FIG. 2. Isotropic and anisotropic TOF profiles of $O(^3P_2)$ products at photolysis wavelength 237 nm: (a) $\mathbf{I}^X_{iso}$, (b) $\mathbf{I}^Z_{iso}$, (c) $\mathbf{I}^X_{aniso}$, (d) $\mathbf{I}^Z_{aniso}$. Experimental data are shown as dashed lines, fitted data are solid lines.

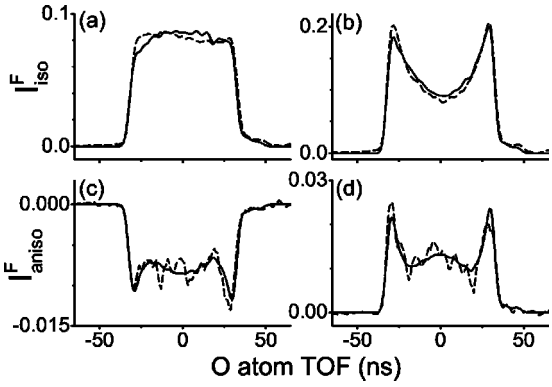

FIG. 3. Isotropic and anisotropic TOF profiles of $O(^3P_1)$ products at photolysis wavelength 222 nm: (a) $\mathbf{I}^X_{iso}$, (b) $\mathbf{I}^Z_{iso}$, (c) $\mathbf{I}^X_{aniso}$, (d) $\mathbf{I}^Z_{aniso}$. Experimental data are shown as dashed lines, fitted data are solid lines.

III. RESULTS

A. Branching ratios

At the fixed photolysis wavelength 226 nm, we measured the total ion intensity for $O(^3P_j)$ atom REMPI for $j=0,1,2$. The ion signals were corrected for variations in probe laser energy. We found the relative branching ratio to be 1.00:2.90:8.65 for $j=0:1:2$. Our results are in good agreement with the branching ratios 1.00 ± 0.26:3.33 ± 0.43:9.00 ± 0.70 reported by Buijsse *et al.*[3] Using branching populations and excitation factors in Tables II and III of VG,[9] we obtain a semiclassical estimate at 226 nm of 1.00:4.32:9.73, which agrees well with the experimental results.

B. Alignment

Isotropic and anisotropic TOF profiles $\mathbf{I}^F_G$ $(F=X,Z)$ are shown in Figs. 1 (222 nm) and 2 (237 nm) for $O(^3P_2)$ products, and Figs. 3 and 4 for $O(^3P_1)$. The resulting alignment parameters are given in Table II, and plotted in Fig. 5. The incoherent parameter $\mathbf{a}^{(2)}_0(\parallel)$ has opposite signs for $j=1$ compared with $j=2$, and the same is true for $\mathbf{a}^{(2)}_0(\perp)$. For a particular j at a given photolysis wavelength, we also find that $\mathbf{a}^{(2)}_0(\parallel)$ and $\mathbf{a}^{(2)}_0(\perp)$ have opposite signs. The $\mathbf{a}^{(2)}_0(\parallel)$ does not appear to change, within uncertainties, from 222 nm compared to 237 nm and the $\mathbf{a}^{(2)}_0(\perp)$ appears to decrease at

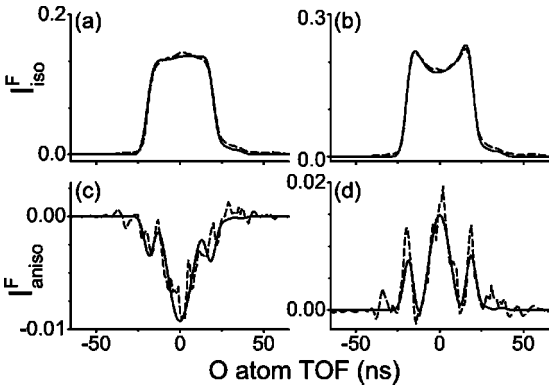

FIG. 4. Isotropic and anisotropic TOF profiles of $O(^3P_1)$ products at photolysis wavelength 237 nm: (a) $\mathbf{I}^X_{iso}$, (b) $\mathbf{I}^Z_{iso}$, (c) $\mathbf{I}^X_{aniso}$, (d) $\mathbf{I}^Z_{aniso}$. Experimental data are shown as dashed lines, fitted data are solid lines.

TABLE II. Experimental beta parameters (β) and molecule frame alignment parameters $\mathbf{a}_q^{(2)}(p)$ for $O(^3P_j)$ atoms at photolysis wavelengths 222 and 237 nm. The calculated semiclassical $\mathbf{a}_0^{(2)}(p)$ from Table III are also shown here for convenience. The calculated $\mathrm{Re}[\mathbf{a}_1^{(2)}(\parallel,\perp)]$ and $\mathbf{a}_2^{(2)}(\perp)$ were obtained using methods outlined in Sec. III C.

	$j=1$		$j=2$	
Parameter	222 nm	237 nm	222 nm	237 nm
β	0.51 ± 0.10	0.25 ± 0.15	0.55 ± 0.10	0.50 ± 0.10
$\mathbf{a}_0^{(2)}(\parallel)$	$+0.158\pm0.043$	$+0.123\pm0.048$	-0.090 ± 0.037	-0.125 ± 0.030
calculated	$+0.055$	-0.007	-0.060	-0.191
$\mathbf{a}_0^{(2)}(\perp)$	-0.223 ± 0.071	-0.052 ± 0.057	$+0.081\pm0.066$	$+0.015\pm0.050$
calculated	-0.131	-0.048	$+0.073$	$+0.000$
$\mathrm{Re}[\mathbf{a}_1^{(2)}(\parallel,\perp)]$	-0.115 ± 0.042	$+0.069\pm0.035$	$+0.090\pm0.037$	-0.001 ± 0.027
calculated			-0.348	-0.036
$\mathbf{a}_2^{(2)}(\perp)$	$+0.019\pm0.035$	$+0.061\pm0.023$	-0.094 ± 0.033	-0.009 ± 0.021
calculated			-0.086	-0.049

longer wavelengths for both j, most significantly for $j=1$. The coherent parameter $\mathbf{a}_2^{(2)}(\perp)$ is positive for $j=1$ and negative for $j=2$, at both wavelengths.[20]

Currently there have been no theoretical estimates of the effects of coherence on the atomic alignment for dissociation of O_2. Balint–Kurti *et al.*[21] have recently reported an *ab initio* study of the dissociation of HF, in which they used a time-dependent wave packet approach to obtain the photofragmentation matrix, **T**. The **T** matrix elements contain the phase and amplitude information that is required for calculation of the coherent polarization parameters $\mathrm{Re}[\mathbf{a}_1^{(2)}(\parallel,\perp)]$ and $\mathbf{a}_2^{(2)}(\perp)$, and a similar study for the O_2 system would allow a detailed comparison with our experimental results. We have, however, made approximate semiclassical calculations of these coherent alignment moments for $j=2$ atoms, using Eqs. (12)–(14) as outlined in Sec. III C. We found a large discrepancy between the experimental and semiclassical $\mathrm{Re}[\mathbf{a}_1^{(2)}(\parallel,\perp)]$ at 222 nm. Overall, however, the agreement between the semiclassical and experimental coherent alignment parameters is good.

The molecule frame alignment tensor moments $\rho_0^{(2)}$ calculated by VG (Ref. 9) can be related to the molecule frame alignment parameters $\mathbf{a}_0^{(2)}(\parallel)$ and $\mathbf{a}_0^{(2)}(\perp)$ of Rakitzis *et al.*,[10]

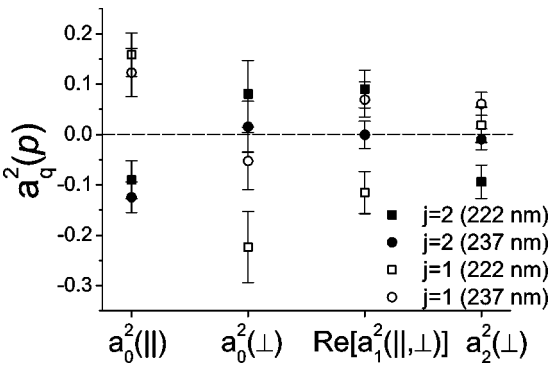

FIG. 5. Molecule frame alignment parameters $\mathbf{a}_q^{(2)}(p)$ for $O(^3P_j)$ atoms at 222 nm (squares) and 237 nm (circles). Solid symbols are $j=2$ atoms, open symbols are $j=1$ atoms.

$$\mathbf{a}_0^{(2)}=\left[\frac{(2j-1)(2j+1)(2j+3)}{5j(j+1)}\right]^{1/2}\rho_0^{(2)}. \tag{9}$$

The semiclassical calculations of VG were obtained at energies equivalent to photolysis wavelengths 204, 216, 226, 236, and 240 nm and our experimental results were obtained at 221.667 and 237.049 nm. We have made linear interpolations of the results of VG in order to compare with our experimental data: these were calculated as $\rho_0^{(2)}(222\,\mathrm{nm})=0.5667\times\rho_0^{(2)}(226\,\mathrm{nm})+0.4333\times\rho_0^{(2)}(216\,\mathrm{nm})$, and $\rho_0^{(2)}(237\,\mathrm{nm})=0.7377\times\rho_0^{(2)}(236\,\mathrm{nm})+0.2623\times\rho_0^{(2)}(240\,\mathrm{nm})$. The resulting $\rho_0^{(2)}$ were converted to $\mathbf{a}_0^{(2)}$, using Eq. (9), and are given in Table III. Also shown in Table III are interpolated semiclassical excitation branching ratios to each of the Herzberg states, and their respective β parameters.

From Table III we see that dissociation via $A\ ^3\Sigma_{u,\pm1}^+$ has both parallel and perpendicular contributions. For example, if $\beta=1.219$ we determine that $(\beta+1)/3=0.740$ is the parallel branching fraction of the $A\ ^3\Sigma_{u,\pm1}^+$ state dissociation at 222 nm. The total parallel branching fraction for O_2 dissociation at 222 nm is $0.735\times0.740=0.544$. From Table III, $\mathbf{a}_0^{(2)}(j=2)=-0.111$ for the $A\ ^3\Sigma_{u,\pm1}^+$ state at 222 nm. We calculate the total parallel contribution to alignment as $\mathbf{a}_0^{(2)}(\parallel)=-0.111\times0.544=-0.060$. The last two rows in Table III are the weighted sums of the contributions from parallel and perpendicular transitions, and the calculated $\mathbf{a}_0^{(2)}(p)$ results are compared to the experimental results in Table II. Comparing the experimental and calculated $\mathbf{a}_0^{(2)}(p)$ in Table II, we see good quantitative agreement overall, within experimental uncertainties. There appears to be greater discrepancy between experimental and calculated results for $\mathbf{a}_0^{(2)}(\parallel)$, particularly for $j=1$ atoms.

The dissociation of O_2 via the Herzberg continuum approaches the threshold for the $O(^3P)+O(^3P)$ dissociation limit, and we must consider the potential effects of nonaxial recoil. In the $X\ ^3\Sigma_g^-$ electronic state there are only odd rotational J states, with the lowest populated level being $J=1$. The estimated rotational temperature of our expansion is 15 K, and we calculate fractional Boltzmann populations as 0.787, 0.197, and 0.016 for $J=1$, 3, and 5, respectively. The dissociation energy of O_2 is $D_0^0(O_2)=41268.6\ \mathrm{cm}^{-1}$. Assuming dissociation from $O_2(J=1)$ to give two ground state

TABLE III. Herzberg excitation branching ratios $p_{n\Omega}$ and state-specific anisotropy parameters $\beta_{n\Omega}$ for different molecular eigenstates, calculated from Table II of VG (Ref. 9). Semiclassical alignment parameters $\mathbf{a}_0^{(2)}(j=1,2)$ were calculated by interpolation from the results of VG, see text for details.

State	$p_{n\Omega}$		$\beta_{n\Omega}$		$\mathbf{a}_0^{(2)}(j=1)$		$\mathbf{a}_0^{(2)}(j=2)$	
	222 nm	237 nm	222 nm	237 nm	222 nm	237 nm	222 nm	237 nm
$A\ ^3\Sigma_{u,1}^+$	0.735	0.727	1.219	1.253	0.102	−0.012	−0.111	−0.350
$A\ ^3\Sigma_{u,0}^+$	0.191	0.181	−1	−1	−0.648	−0.154	0.378	0.235
$c\ ^1\Sigma_{u,0-}^-$	0.021	0.027	−1	−1	0.174	0.254	0.435	0.271
$A'\ ^3\Delta_{u,1}$	0.021	0.026	−1	−1	−0.244	−0.254	−0.492	−0.278
$A'\ ^3\Delta_{u,2}$	0.031	0.039	−1	−1	−0.824	−0.482	0.720	0.531
$A'\ ^3\Delta_{u,3}$	0.001	0.001	−1	−1	0.500	0.500	0.436	0.377
total $\parallel$	0.544	0.546	+2	+2	0.055	−0.007	−0.060	−0.191
total $\perp$	0.456	0.454	−1	−1	−0.131	−0.048	0.073	0.000

$O(^3P_2)$ atoms, we estimate the final center-of-mass velocity of O atoms to be 1681 m s^{-1} at 222 nm and 832 m s^{-1} at 237 nm. Following Wrede *et al.*[20] we calculated the total quasiclassical angle of rotation γ that accumulates during the dissociation, i.e., γ is the angle between the asymptotic velocity vector of the O atoms and the position of the internuclear axis at the time of excitation. For $O_2(J=1)$ we find that $\gamma=1.4°$ at 222 nm and $\gamma=2.5°$ at 237 nm, and for O_2 $(J=3)$ $\gamma=3.5°$ at 222 nm and $\gamma=6.2°$ at 237 nm. The effect of these deviations from axial recoil are small: for $\gamma=6.2°$ β would be degraded to only 0.98 of its axial value.[20]

A further complication in our experiment is that we are unable to determine the *correlated* alignment between $\boldsymbol{j}_A$ and $\boldsymbol{j}_B$ for the two atoms, so there is an implicit averaging over the co-fragment with $j=0,1,2$. The energy separation ~ 100 cm^{-1} between j levels of $O(^3P)$ would make it very challenging to obtain correlated experimental data. It is possible, however, that the effects of the implicit averaging could be assessed in future calculations.

In summary, the semiclassical $\mathbf{a}_0^{(2)}$ of VG agree well with our experimental results. We expect that a fully quantum model of the Herzberg excitation and dissociation, which could include calculation of the coherent alignment parameters, would improve the agreement between theory and experiment.[22]

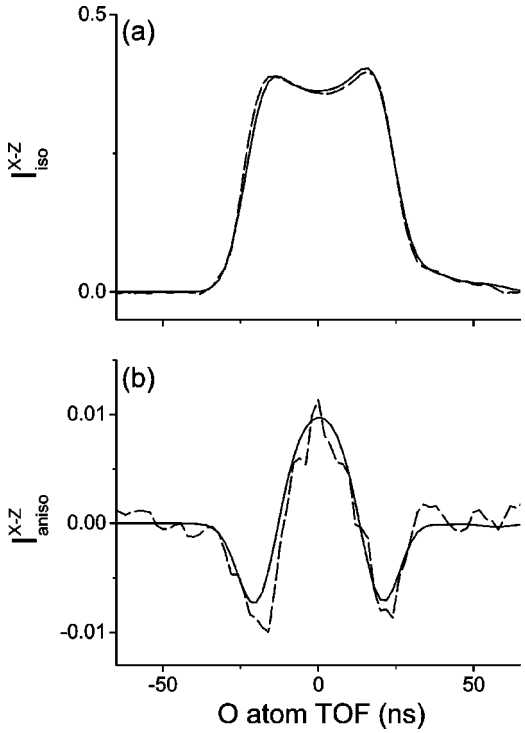

FIG. 6. Isotropic and anisotropic TOF profiles of $O(^3P_2)$ products at photolysis wavelength 223.543 nm: (a) $\mathbf{I}_{\rm iso}^{X-Z}$, (b) $\mathbf{I}_{\rm aniso}^{X-Z}$. Experimental data are shown as dashed lines, fitted data are solid lines.

C. Orientation

Typical isotropic and anisotropic TOF profiles $\mathbf{I}_G^{X-Z}$ at photolysis wavelength 223.543 nm are shown in Fig. 6. The resulting $\mathrm{Im}[\mathbf{a}_1^{(1)}(\parallel,\perp)]$ obtained from measurements over a range of photolysis wavelengths 218.521–238.556 nm are shown in Fig. 7, and tabulated in Table IV. The $\mathrm{Im}[\mathbf{a}_1^{(1)}(\parallel,\perp)]$ parameter represents orientation along the molecule-frame y axis resulting from interference between states of parallel and perpendicular symmetry.[10] The $\mathrm{Im}[\mathbf{a}_1^{(1)}(\parallel,\perp)]$ contains both amplitude and phase information. For the simple case of interference between two states (one parallel, one perpendicular) we can write

$$\mathrm{Im}[\mathbf{a}_1^{(1)}(\parallel,\perp)]\propto \sin\Delta\phi, \tag{10}$$

where $\sin(\Delta\phi)=\sin(\phi_\perp-\phi_\parallel)$ is the sine of the asymptotic phase difference between the radial parts of the dissociative wave functions for the perpendicular and parallel states. The photodissociation of O_2 involves more than one pair of interfering electronic states. A fully quantum mechanical simulation of the dissociation is outside the scope of the present study. However, as a base to compare with our experimental results, we have calculated the energy dependence of the semiclassical phase difference using the O_2 potential energy curves of VG.[8]

We begin by writing the $\mathrm{Im}[\mathbf{a}_1^{(1)}(\parallel,\perp)]$ in terms of the dynamical functions $f_k(q,q')$ of Siebbeles *et al.*[17]

$$\mathrm{Im}[\mathbf{a}_1^{(1)}(\parallel,\perp)]=-\frac{6\ \mathrm{Im}[f_1(1,0)]}{\sqrt{2}[f_0(0,0)+2f_0(1,1)]}. \tag{11}$$

The dynamical functions can be written as[21]

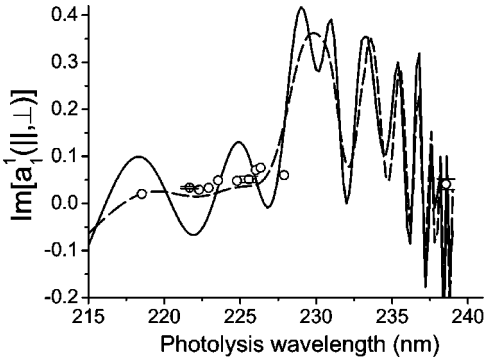

FIG. 7. Molecule frame orientation parameter $\mathrm{Im}[\mathbf{a}_1^{(1)}(\parallel,\perp)]$ for $O(^3P_2)$ atoms vs photolysis wavelength. Circles are experimental points. The solid line is the semiclassical simulation obtained using potential energy curves of VG [see Eq. (15) (Ref. 8)]. The dashed line incorporates a reduction in the term involving the $c0$ state. See text for details.

$$f_k(q,q')=\sum_{n,\Omega,\Omega_A,n',\Omega',\Omega_A'}(-1)^{k+j_A+\Omega_A'}\times\begin{pmatrix} j_A & j_A & k \\ -\Omega_A & \Omega_A' & q-q' \end{pmatrix}\times\mathcal{T}^{n\Omega}_{j_A\Omega_A j_B\Omega_B}(\mathcal{T}^{n'\Omega'}_{j_A\Omega_A' j_B\Omega_B})^*\times r^*_{n\Omega}r_{n'\Omega'}e^{-i\phi_{n\Omega}}e^{i\phi_{n'\Omega'}}, \tag{12}$$

where we have combined Eqs. (6) and (13) of Ref. 21. The dissociation gives two fragments with angular momenta j_A and j_B, having projections Ω_A and Ω_B on the molecule frame z axis. The indices $n\Omega$ label the excited state with $\Omega=\Omega_A+\Omega_B$. To be brief, we shall refer to the six Herzberg states of Table III as $A1$, $A0$, $c0$, $A'1$, $A'2$, and $A'3$. As explained by Balint–Kurti *et al.*, summation over Ω_B is implicitly included in Eq. (12), and $q-q'=\Omega_A-\Omega_A'=\Omega-\Omega'$. The coefficients $\mathcal{T}^{n\Omega}_{j_A\Omega_A j_B\Omega_B}$ are expansion coefficients of the molecular electronic states in the product atomic basis $|j_A\Omega_A\rangle|j_B\Omega_B\rangle$, which can be calculated by diagonalizing the long-range quadrupole–quadrupole potential interaction matrix in the atomic basis. $\mathcal{T}^{n\Omega}_{j_A\Omega_A j_B\Omega_B}$ coefficients for O_2 have been given in Table I of VG.[9]

The dynamical function $f_1(1,0)$ represents a sum over $(\parallel,\perp)$ pairs of interfering states. No interference occurs between dissociation paths that start with different values of the ground state Ω_i. Since the only parallel transition involved is from ground state $X1\rightarrow A1$ [see Eq. (2)], the only perpendicular transitions to be considered in $f_1(1,0)$ are $X1\rightarrow A0$, $c0$, and $A'2$.

The coefficients $r_{n\Omega}$ and $\phi_{n\Omega}$ in Eq. (12) are amplitudes and phases of the photofragment **T** matrix. For their work on HF photodissociation,[21] Balint–Kurti *et al.* calculated the **T** matrix from time-dependent wave-packet dynamical calculations. In the present case, we approximate by using the semiclassical results of VG to obtain amplitudes as the (positive) root of the branching ratios in Table III. For parallel transitions $r_{n\Omega}=(p_{n\Omega})^{1/2}$, and for perpendicular transitions $r_{n\Omega}=(p_{n\Omega}/2)^{1/2}$. The branching ratios $p_{n\Omega}$ depend on the photolysis wavelength, and are given in Table II of Ref. 9. The parallel component $p_{A1\parallel}=p_{A1}\times(1+\beta)/3$ of the branching fraction to $A1$ has been used. Taking the positive root we have introduced a factor of π uncertainty in the phase for each pair of interfering states in $f_1(1,0)$.

TABLE IV. Experimental molecule frame orientation parameters $\mathrm{Im}[\mathbf{a}_1^{(1)}(\parallel,\perp)]$ for $O(^3P_2)$ atoms.

Wavelength (nm)	$\mathrm{Im}[\mathbf{a}_1^{(1)}(\parallel,\perp)]$
218.521	0.020
221.667	0.034 ± 0.002
222.293	0.030
222.918	0.033
223.543	0.049
224.789	0.048
225.566	0.052 ± 0.007
226.031	0.071
226.341	0.076
227.888	0.060
238.556	0.041 ± 0.011

The total semiclassical phase ϕ_n for state $n\equiv n\Omega$ was found by numerical integration using the adiabatic Hund's case (c) potential energy curves of VG with the expression[23]

$$\phi_n=\frac{\pi}{4}+\int_{T_n}^{\infty}[k_n(R)-k_n(\infty)]\mathrm{d}R-k_n(\infty)T_n, \tag{13}$$

where R is the O_2 bond length, T_n is the classical inner turning point for state n at a given available energy E. The available energy $E=h\nu-D_0^0(O_2)$, where $h\nu$ is the energy of the photolysis photon. The de Broglie wave number $k_n(R)$ is

$$k_n(R)=\frac{1}{\hbar}\sqrt{2\mu\{E-E_n(R)\}}, \tag{14}$$

where μ is the reduced mass of O_2, and $E_n(R)$ is the potential energy of state n. The centrifugal potential due to rotation of the dissociating O_2 was found to be insignificant in our calculations and has not been included in Eq. (14). The case (c) potentials were obtained by diagonalization of the matrix elements of the Hamiltonian $\hat{H}=\hat{H}_{\mathrm{Coul}}+\hat{H}_{\mathrm{SO}}$ in the basis of the electronic states for $\Omega=0$, 1, 2, and 3, respectively, as a function of the internuclear separation, R. The eigenvalues of the Coulombic Hamiltonian $\hat{H}_{\mathrm{Coul}}$ correspond to the electronic adiabatic Born–Oppenheimer (ABO) states, and the matrix elements of $\hat{H}_{\mathrm{SO}}$ are the spin–orbit couplings between ABO states.[24]

Equations (11)–(14) show how $\mathrm{Im}[\mathbf{a}_1^{(1)}(\parallel,\perp)]$ is related to the potential energy curves $E_n(R)$ through the phase accumulated during dissociation at a given available energy E. When the available energy is much larger than the potential energy difference between parallel and perpendicular curves, the phase difference $\Delta\phi$ does not vary much, and the $\mathrm{Im}[\mathbf{a}_1^{(1)}(\parallel,\perp)]$ will change very slowly as a function of the photolysis energy. Nearer to threshold, however, $\Delta\phi$ varies more rapidly with E, and measurement of the energy dependence of $\mathrm{Im}[\mathbf{a}_1^{(1)}(\parallel,\perp)]$ can be a very sensitive test of the shapes of the potential energy curves.[25] For the present case, we calculate

$$\mathrm{Im}[\mathbf{a}_1^{(1)}(\parallel,\perp)] = f_{A0} r_{A0} r_{A1\parallel} \sin(\Delta\phi_{A0}) + f_{c0} r_{c0} r_{A1\parallel} \sin(\Delta\phi_{c0}) + f_{A'2} r_{A'2} r_{A1\parallel} \sin(\Delta\phi_{A'2}), \quad (15)$$

where $\sin(\Delta\phi_{n\Omega}) \equiv \sin(\phi_{n\Omega} - \phi_{A1})$ and the constants $f_{A0} = -1.060$, $f_{c0} = -1.325$, and $f_{A'2} = -1.458$. Recall that we have no knowledge about the sign of each term in Eq. (15). We have therefore chosen the coefficients $f_{n\Omega}$ to have the same sign, which qualitatively matches the experimental data. The results of the semiclassical calculation of Eq. (15) are shown as the solid line in Fig. 7. Even with uncertainty in the relative signs of the three terms in Eq. (15), the magnitude of the calculated $\mathrm{Im}[\mathbf{a}_1^{(1)}(\parallel,\perp)]$ is remarkably close to the experimental points. There are pronounced ripples in the orientation: the frequency of the ripples increase at longer wavelength, as the available energy decreases on approach to the threshold. At wavelengths around 225 nm, the magnitude of oscillation in the calculated orientation is larger than experimentally observed. The oscillations in this energy region are mostly due to the interference component involving the $c0$ state. By fitting the experimental data using a nonlinear least-squares algorithm, we investigated the effect of reducing the contribution from the $c0$ state. We find that the experimental results are more closely followed if the contribution from the $c0$ state is reduced by multiplying the second term in Eq. (15) by a constant factor of 0.15. The resulting orientation is shown as the dashed curve in Fig. 7. The reduction factor is equivalent to reducing the branching fraction p_{c0} in Table III at 222 nm from 0.021 to 4.5×10^{-4}. This is a sizable reduction, and it is very doubtful that this is the sole source of discrepancy between the experiment and our semiclassical calculations. Unfortunately, the maximum observed in the calculated results at around 230 nm can only be inferred in our experimental data as it covers a region that was difficult to access with our photolysis nonlinear mixing setup. Despite the simplicity of our semiclassical calculations, the results show reasonable agreement with the experimental results.

IV. CONCLUSIONS

We have made a detailed study of the $O(^3P_j)$ atom alignment and orientation following photodissociation of O_2 in the Herzberg continuum in the region 218–239 nm. The polarization parameter formalism used has allowed us to determine alignment contributions from parallel or perpendicular transitions, and alignment resulting from coherence between excited dissociative states. Experimental alignment parameters were found to be in reasonably good agreement with recent semiclassical simulations by van Vroonhoven and Groenenboom (VG). We have found that photolysis with linearly polarized light produces oxygen atoms that are oriented as a result of interference between multiple excited dissociative states of parallel and perpendicular symmetry. The photolysis energy dependence of the orientation can be related to the phase difference between parallel and perpendicular states. Semiclassical calculations of the energy-dependent orientation were made using Hund's case (c) potential energy curves of VG, and were shown to give good agreement with the experimental results.

The photodissociation of O_2 via the Herzberg continuum reveals a surprisingly rich photochemistry involving motions on—and interactions between—more than one electronic potential energy surface that correlates to the separated open-shell atomic photofragments. This work brings out the inadequacy of the Born–Oppenheimer approximation in describing the dissociation of simple molecules when the dissociating state lies in the midst of other excited states of different symmetry. The Herzberg continuum serves as a fundamental example of nonadiabatic photodissociation. As further theoretical studies are carried out, we hope that our experimental results will provide additional tests for our understanding of this important atmospheric process.

ACKNOWLEDGMENTS

The authors thank Mirjam van Vroonhoven and Gerrit Groenenboom for helpful discussions about their work, and Félix Fernández-Alonso for useful discussions about oxygen atom REMPI. Z.H.K. gratefully acknowledges receipt of a Dr. Franklin Veatch Memorial Fellowship. This work was funded by the National Science Foundation under Grant No. CHE-99-00305.

[1] D. H. Parker, Acc. Chem. Res. **33**, 563 (2000).
[2] W. B. DeMore, S. P. Sander, D. M. Golden, R. F. Hampson, M. J. Kurylo, C. J. Howard, A. R. Ravishankara, C. E. Kolb, and M. Molina, JPL Publication 97-4, 1997.
[3] B. Buijsse, W. J. van der Zande, A. T. J. B. Eppink, D. H. Parker, B. R. Lewis, and S. T. Gibson, J. Chem. Phys. **108**, 7229 (1998).
[4] R. N. Zare and D. R. Herschbach, Proc. IEEE **51**, 173 (1963).
[5] Y. Matsumi and M. Kawasaki, J. Chem. Phys. **93**, 2481 (1990).
[6] Y. -L. Huang and R. J. Gordon, J. Chem. Phys. **94**, 2640 (1991).
[7] K. Tonokura, N. Shafer, Y. Matsumi, and M. Kawasaki, J. Chem. Phys. **95**, 3394 (1991).
[8] M. C. G. N. van Vroonhoven and G. C. Groenenboom, J. Chem. Phys. **116**, 1954 (2002).
[9] M. C. G. N. van Vroonhoven and G. C. Groenenboom, J. Chem. Phys. **116**, 1965 (2002).
[10] T. P. Rakitzis and R. N. Zare, J. Chem. Phys. **110**, 3341 (1999).
[11] T. P. Rakitzis, S. A. Kandel, A. J. Alexander, Z. H. Kim, and R. N. Zare, J. Chem. Phys. **110**, 3351 (1999).
[12] W. R. Simpson, A. J. Orr-Ewing, S. A. Kandel, T. P. Rakitzis, and R. N. Zare, J. Chem. Phys. **103**, 7299 (1995).
[13] A. J. Orr-Ewing and R. N. Zare, Annu. Rev. Phys. Chem. **45**, 315 (1994).
[14] R. N. Zare, *Angular Momentum: Understanding Spatial Aspects in Physics and Chemistry* (Wiley, New York, 1988).
[15] Y. Mo and T. Suzuki, J. Chem. Phys. **109**, 4691 (1998).
[16] P. C. Samartzis, B. L. G. Bakker, T. P. Rakitzis, D. H. Parker, and T. N. Kitsopoulos, J. Chem. Phys. **110**, 5201 (1999).
[17] L. D. A. Siebbeles, M. Glass-Maujean, O. S. Vasyutinskii, J. A. Beswick, and O. Roncero, J. Chem. Phys. **100**, 3610 (1994).
[18] B. V. Picheyev, A. G. Smolin, and O. S. Vasyutinskii. J. Phys. Chem. A **101**, 7614 (1997); A. S. Bracker, E. R. Wouters, A. G. Suits, and O. S. Vasyutinskii, J. Chem. Phys. **110**, 6749 (1999).
[19] A. J. Alexander, J. Chem. Phys. **118**, 6234 (2003).
[20] E. Wrede, E. R. Wouters, M. Beckert, R. N. Dixon, and M. N. R. Ashfold,

J. Chem. Phys. **116**, 6064 (2002).
[21] G. G. Balint–Kurti, A. J. Orr-Ewing, J. A. Beswick, A. Brown, and O. S. Vasyutinskii, J. Chem. Phys. **116**, 10760 (2002).
[22] M. C. G. N. van Vroonhoven and G. C. Groenenboom (personal communications).
[23] Y. Asano and S. Yabushita, J. Phys. Chem. A **105**, 9873 (2001).
[24] M. C. G. N. van Vroonhoven and G. C. Groenenboom, J. Chem. Phys. **117**, 5240 (2002).
[25] T. P. Rakitzis, S. A. Kandel, A. J. Alexander, Z. H. Kim, and R. N. Zare, Science (Washington, D.C., U.S.) **281**, 1346 (1998).